

Superstructure of Challis mordenite with doubled monoclinic unit cell

NAOYUKI KAWAME,^{1,*} DAIJO IKUTA,¹ HIDEKI KANAZAWA,¹ KAZUHIKO ITO,² MICKEY E. GUNTER,³
MONTE B. BOISEN,⁴ AND OSAMU TAMADA¹

¹Graduate School of Human and Environmental Studies, Kyoto University, Sakyo-ku, Kyoto 606–8501, Japan

²Department of Bio-Environmental Sciences, Kyoto Gakuen University, Sogabecho-Kameoka, Kyoto 621–8555, Japan

³Department of Geological Sciences, University of Idaho, Moscow, Idaho 83844-3022, U.S.A.

⁴Department of Mathematics, University of Idaho, Moscow, Idaho 83844-1103, U.S.A.

ABSTRACT

A new superstructure was found in mordenite ($\text{Na}_{5.59}\text{Ca}_{1.80}\text{Al}_{9.19}\text{Si}_{38.81}\text{O}_{96}\cdot n\text{H}_2\text{O}$) from Challis Valley, Idaho—a zeolite widely used in previous studies. The occurrence of the superstructure reflections were observed in 12 specimens from two rock samples, at the midpoint of layers in the oscillation photographs around the \mathbf{a}^* and \mathbf{b}^* axes, but not around the \mathbf{c}^* axis. The apparent $2\mathbf{a}$, $2\mathbf{b}$, and \mathbf{c} axes are orthogonal. In spite of yielding an apparent orthorhombic cell, careful observation of the intensities revealed that the superstructure is monoclinic with twice the volume of the orthorhombic cell: $a' = 27.356(9)$, $b' = 27.356(9)$, $c' = 7.517(2)$ Å, $\gamma' = 97.14(4)^\circ$, and $V' = 5582(4)$ Å³.

The presence of the superstructure was examined for specimens from ten other localities and a synthetic sample but there was no evidence for extra spots of the superstructure, indicating that the occurrence is not common.

The large displacement factors of O8 oxygen, and its associated 180° T-O-T angle that is energetically unfavorable, are basic to the mordenite structure. In the monoclinic superstructure the O8 oxygen is decomposed into several asymmetric O atoms by the symmetry reduction. The large displacement smearing of O8 oxygen perpendicular to the straight T-O-T, are explained by the superposition of decomposed O atoms.

The extra spots are predominantly observed in the reciprocal planes with $l = \text{odd}$ in the same way as diffuse streaks. The observation of extra spots and diffuse streaks suggests that there are three kinds of domains in the mordenite, one in the ordered form and two others in the random form of $c/2$ linear displacements. The domain in the ordered form represents the superstructure. Thus, we propose a model for the superstructure in which the $c/2$ displacement occurs alternatively in the two basic unit cells slightly modified in the superstructure, yielding the periodic arrangements.

Keywords: Mordenite, superstructure, monoclinic cell, diffuse streak, linear displacement, ordered form

INTRODUCTION

Mordenite, ideally $\text{Na}_8\text{Al}_8\text{Si}_{40}\text{O}_{96}\cdot 24\text{H}_2\text{O}$, is a member of zeolite group with the most siliceous composition of any zeolite. Its structure is characterized by 12-membered and 8-membered rings running along the \mathbf{c} axis, and another 8-membered rings running along the \mathbf{b} axis; these channels accommodate extraframework cations and water molecules. The mineral, especially synthetic varieties, has many industrial applications such as isomerization catalysts. The structure has an orthorhombic unit cell ($a = 18.1$ Å, $b = 20.5$ Å, and $c = 7.5$ Å) with topological space group symmetry $Cmcm$. Meier (1961) first determined the crystal structure of a Na-exchanged mordenite from Challis Valley, Idaho in $Cmcm$ space group, suggesting that the ordered Al/Si distributions would reduce the symmetry to acentrosymmetrical $Cmc2_1$. After Meier's determination, several structural analyses were performed for both natural and synthetic mordenites as summarized by Armbruster and Gunter (2001).

In the course of these studies, several additional space groups for different polytypes of mordenite-related structures have been proposed, such as: $Immm$, $Cmmm$, and $Imcm$ (Kerr 1963; Sherman and Bennett 1973), but these hypothetical space groups were determined to be experimental artifacts resulting from diffuse halos of adjacent layers (Simoncic and Armbruster 2004a). Current research indicates that the original $Cmcm$ and $Cmc2_1$ are the correct space group for mordenite; however, dehydrated, cation-exchanged forms occur with $Pbcn$ space group (Mortier et al. 1978; Schlenker et al. 1978, 1979). The structures of hydrated, cation-, and molecule-exchanged samples (e.g., Se, thionin blue and methylene blue dyes), have been refined in the lower symmetry monoclinic space group Cc because of the better fits but there is no direct experimental evidence for monoclinic symmetry (Simoncic and Armbruster 2004b, 2005; Simoncic et al. 2004).

Diffuse reflections in mordenite have been observed in X-ray and electron diffraction photographs (e.g., Sherman and Bennett 1973; Sanders 1985; Simoncic and Armbruster 2004a). The diffuse scattering extends perpendicular to the \mathbf{c} axis and is restricted

* E-mail: kawame@crystal.mbox.media.kyoto-u.ac.jp

for Bragg reflections $l = \text{odd}$, which leads to the interpretation that linear framework defects displaced by $c/2$ cause the diffuse scattering (Sanders 1985; Campbell and Cheetham 2002). Rudolf and Garcés (1994) also concluded from an X-ray powder diffraction (XRPD) study that the c -axis faulted structure accounts for the observed XRPD behavior. Campbell et al. (2004) mapped out the distributions of diffuse scattering using a synchrotron X-ray source with a CCD detector and demonstrated an excellent match with a simulated diffuse scattering pattern. In accordance with these observations of diffuse reflections, the presence of domains displaced by $c/2$ was directly seen in the difference Fourier maps (Mortier et al. 1975; Simoncic and Armbruster 2004a).

Schlenker et al. (1979) determined the crystal structure of dehydrated, Na-exchanged mordenite and showed “splitting of the diffuse streaks into doublets centered on positions with $\approx n \pm 0.4$ ” in Weissenberg photograph of $hk2$ reflections, interpreted as a domain structure with true $a' \approx 5a$. This observation suggests a presence of superstructure in mordenite. Although a number of structural studies for synthetic and natural mordenites have been done by X-ray and electron diffraction methods, and natural mordenite from Challis Valley, Idaho has been widely used for the research specimens (e.g., Meier 1961; Sherman and Bennett 1973; Mortier et al. 1975, 1978; Schlenker et al. 1978, 1979), there is no report of the presence of a superstructure. Here we report the evidence of superstructure in mordenite from Challis Valley, Idaho, which is not orthorhombic, but monoclinic with unique c axis, and twice the volume of the C-centered orthorhombic unit cell (hereafter referred to as the “basic unit cell”).

SAMPLE SELECTION AND EXPERIMENTAL METHODS

Mordenite samples were collected by the authors (Kawame and Gunter) at a site near Challis in Challis Valley, Idaho; this is the site referred to by Ross and Shannon (1924). A needle-like single crystal ($0.41 \times 0.10 \times 0.05$ mm) was used for the X-ray diffraction experiments. The chemical composition was determined by an electron probe micro-analyzer (JOEL JSM-5400) equipped with the energy dispersive X-ray spectrometry EDX (Link QX2000) operated at 15 kV and 0.1 nA. Albite was used as standard for Na, wollastonite for Ca and Si, K-feldspar for K, and sillimanite for Al. The chemical formula obtained was $\text{Na}_{5.59}\text{Ca}_{1.80}\text{Al}_{9.19}\text{Si}_{38.81}\text{O}_{96} \cdot n\text{H}_2\text{O}$, which indicates that the specimen is fairly rich in aluminum.

X-ray diffraction studies were performed on two separate four-circle diffractometers, one equipped with a CCD detector and the other a scintillation point counter (Enraf-Nonius Kappa CCD and Enraf-Nonius MACH3 diffractometers, respectively) using X-ray radiation (50 kV and 30 mA) generated by the sealed MoK α tube. All the experiments were done at room temperature. The X-ray data for the determination of the basic structure were taken with the CCD type diffractometer and were reduced by Denzo-SMN software package (Otwinowski and Minor 1997). The crystal structure was refined to $R(F) = 0.056$ by the program SHELXL-97 (Sheldrick 1997) in the WinGX suite of program (Farrugia 1999) and the figures were drawn by XTALDRAW (Bartelmehs et al. 1993). The cell parameters of this specimen determined using 20 reflections are: $a = 18.111(3)$, $b = 20.467(3)$, $c = 7.522(1)$ Å, and $V = 2788.3(7)$ Å³. Crystal data and experimental conditions are summarized in Table 1.

RESULTS

Presence of superstructure

Oscillation photographs taken around a^* , b^* , and c^* axes using the CCD type diffractometer are shown in Figure 1. In Figure 1a the layers of main reflections are seen at the interval of a^* indicated as layers, $h = 1, 2, 3, \dots$, but in addition to these reflections extra spots are clearly observed at the mid-point of layers as $h = 0.5, 1.5, 2.5, \dots$, and marked by white arrows. This

TABLE 1. Crystal data and experimental conditions

Crystal size (mm)	0.41 × 0.10 × 0.05	
Chemical composition	$\text{Na}_{5.59}\text{Ca}_{1.80}\text{Al}_{9.19}\text{Si}_{38.81}\text{O}_{96} \cdot n\text{H}_2\text{O}$	
Cell dimensions	basic structure	superstructure
a (Å)	18.111(3)	27.356(9)
b (Å)	20.467(3)	27.356(9)
c (Å)	7.522(1)	7.517(2)
γ (°)	90	97.14(4)
V (Å ³)	2788.3(7)	5582(4)
X-ray radiation	MoK α	
Temperature (K)	298	
Absorption correction method	Numerical	
Absorption coefficient μ (mm ⁻¹)	0.76*	
Scan type for MACH3	ω scans	
Scan width for MACH3 (°)	1.35 + 0.53 tan θ	

* In calculation of micrometers, the number of water molecules was fixed to 28.

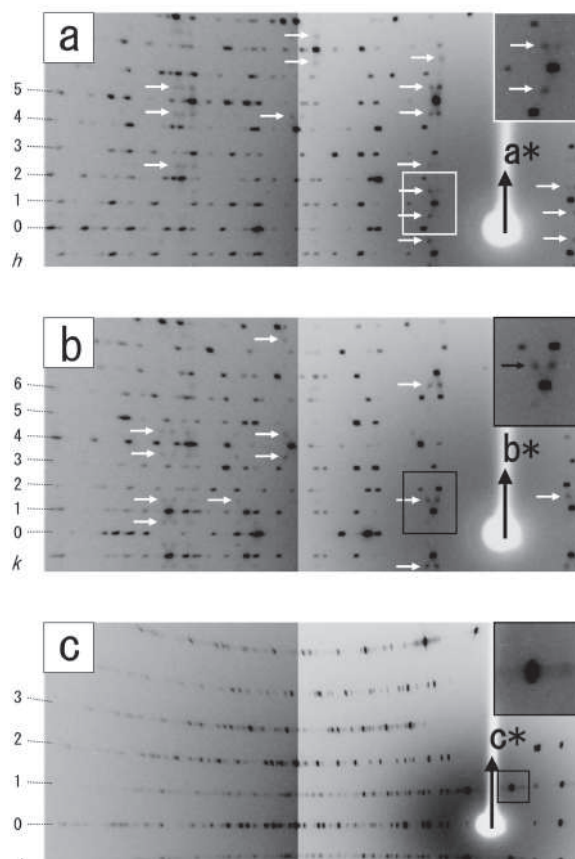


FIGURE 1. Oscillation photographs around (a) a^* , (b) b^* , and (c) c^* axes, taken with the CCD type diffractometer. The gray scale on the left half of photographs is increased to the darker image to emphasize weak spots. Oscillation angles are 90° for a^* and b^* axes and 40° for c^* axis. Some of the extra spots located at the mid-point of layers of main reflections are highlighted by white arrows.

is also true for the b^* oscillation photograph shown in Figure 1b. The extra spots are also observed at the mid-point of layers as $k = 0.5, 1.5, 2.5, \dots$. On the other hand, there are no extra spots in the oscillation photograph around c^* (Fig. 1c). These extra reflections are evidence for the presence of superstructure with the apparent cell 2a, 2b, and c. In Figure 1c the diffuse streaks are faintly seen perpendicular to the c^* axis at $l = \text{odd}$ layers as previously reported (e.g., Campbell et al. 2004).

Symmetry reduction

Cell parameters of the superstructure were determined using 12 superstructure reflections (i.e., those occurring in non-integer values of h or k) assuming a triclinic cell, yielding: $a = 36.21(1)$, $b = 41.00(2)$, $c = 7.520(3)$ Å, $\alpha = 90.07(4)^\circ$, $\beta = 90.02(2)^\circ$, and $\gamma = 90.01(6)^\circ$, $V = 11162(8)$ Å³. Within errors, this unit cell exhibits orthogonal geometry and has a volume four times that of the basic unit cell ($Cmcm$).

To further examine the symmetry, intensities for ten unique reflections of both basic- and super-structure and their symmetry equivalent reflections, were measured by the diffractometer equipped with a point detector. The data for four of these are shown in Figure 2 with each reflection's intensity normalized to unity for the maximum reflection observed in the set. In the eight symmetry equivalent reflections, each of the first four reflections ($+++$, $--+$, $++-$, and $---$) and each of the second set of four reflections ($+-+$, $-++$, $+--$, and $-+-$) in the figure can be assigned to equivalent reflections in $2/m$ monoclinic symmetry with c unique axis. The main reflections exhibit no systematic difference in the eight intensities equivalent to mmm , but the eight reflections for the superstructure split into two groups, the first four and last four reflections, each of which is assigned to $2/m$ (c unique axis). Other measured reflections that are not shown in the figure also exhibit this same trend. Thus, Figure 2 shows irrefutable evidence that the superstructure is monoclinic.

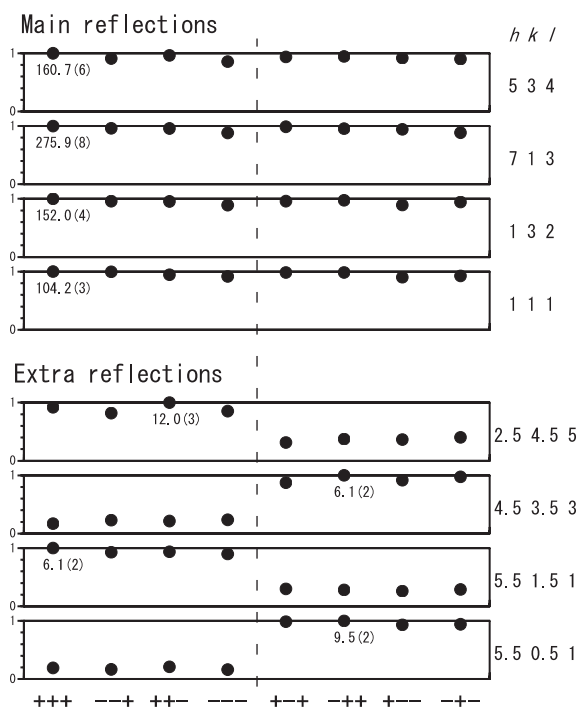


FIGURE 2. Intensity plots of four unique reflections for each of main- and extra-reflections and their symmetry equivalent reflections, normalized to unity for the maximum intensity in the eight mmm equivalent reflections (hkl , $-h-kl$, ..., and $-hk-l$). Intensity measurements were done two times for main reflections and four times for extra reflections, and the final intensities averaged. The standard errors for all the intensities are less than 0.04 (in normalized value). The maximum intensity value for each set is shown with standard error.

The R_{int} values (R -factor for symmetry equivalent reflections) calculated from all the measured intensities are listed in Table 2, in which the R_{int} value exhibits a distinct drop at $112/m$ Laue group for the set of extra reflections. This result also confirms the monoclinic symmetry for the superstructure.

Unit-cell setting for the superstructure

The intensity data of main reflections for the basic structure and extra reflections for the superstructure were collected with the diffractometer equipped with a point detector and are plotted on $hk0$, $hk1$, $hk2$, and $hk3$ reciprocal planes (Fig. 3). From these data the new monoclinic cell for the superstructure was introduced

TABLE 2. R_{int} values (R -factors for symmetry equivalent reflections) for main reflections and extra reflections

	Main	Extra
$2/m\ 1\ 1$	0.036	0.548
$1\ 2/m\ 1$	0.036	0.548
$1\ 1\ 2/m$	0.036	0.053
mmm	0.036	0.542

Note: R_{int} values are calculated from 10 main reflections and 10 extra reflections, and their mmm symmetry equivalents.

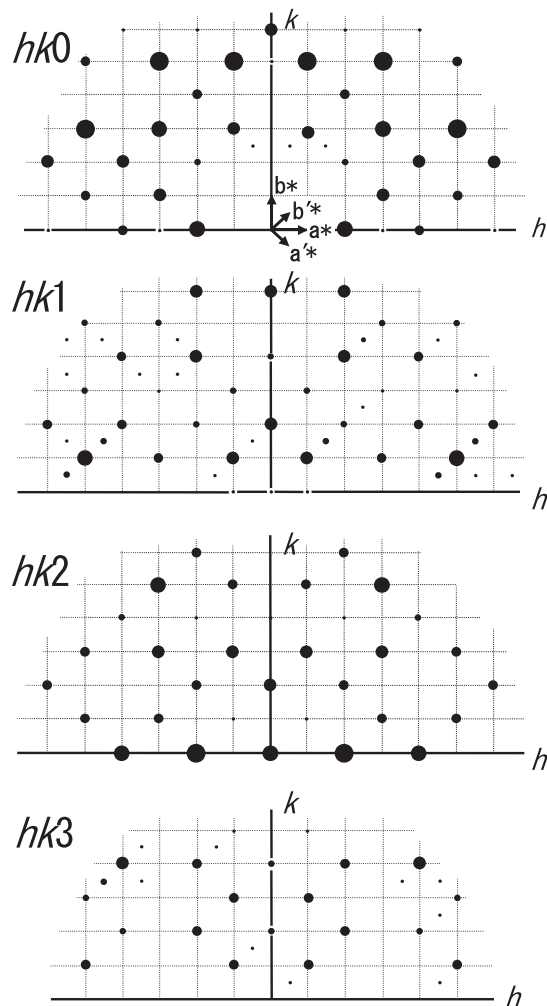


FIGURE 3. Intensity plots of reflections on $hk0$, $hk1$, $hk2$, and $hk3$ reciprocal planes. Reciprocal cell vectors for the basic structure (a^* , b^*) and the superstructure (a^* , b^*) are shown on $hk0$ plane.

in the reciprocal space as $\mathbf{a}^* = (\mathbf{a}^* - \mathbf{b}^*)/2$, $\mathbf{b}^* = (\mathbf{a}^* + \mathbf{b}^*)/2$, and $\mathbf{c}^* = \mathbf{c}^*$ and in real space as $\mathbf{a}' = \mathbf{a} - \mathbf{b}$, $\mathbf{b}' = \mathbf{a} + \mathbf{b}$, and $\mathbf{c}' = \mathbf{c}$ (Fig. 4). The cell parameters for superstructure determined by 12 extra reflections are: $a' = 27.356(9)$, $b' = 27.356(9)$, $c' = 7.517(2)$ Å, $\gamma' = 97.14(4)^\circ$, and $V' = 5582(4)$ Å³. Thus, the cell volume of the superstructure is twice that of basic unit cell. The precision of the cell parameter refinement is somewhat low because of the weak nature of the superstructure reflections.

Distributions of extra spots and space group for the superstructure

The hkl reciprocal lattice planes with $l = \text{even}$ ($hk0$ and $hk2$ in Fig. 3) mostly show no extra reflections for the superstructure. A few exceptions of weak extra reflections occur in the $hk0$ plane, but several extra reflections appear in the planes with $l = \text{odd}$ ($hk1$ and $hk3$ in Fig. 3). This is a characteristic property for the present superstructure, which is similar to the characteristics of diffuse streaks of mordenite. There appears to be no systematic absences and candidates for the space group are Pm , $P2$, and $P2/m$; however, it is difficult to identify systematic absences since the intensities for the superstructure are principally weak.

DISCUSSION

We have shown for the first time that there is a superstructure in the natural Challis mordenite, which has been commonly used in studies on mordenite. We examined twelve specimens from two rock samples and found the extra reflections originated from the superstructure in all the specimens, which demonstrates that the superstructure in Challis mordenites is not confined to an isolated specimen. Thus, it is expected that the superstructure is present in other natural and perhaps synthetic samples. We examined the presence of superstructure in other specimens, but results for specimens from eight localities in Japan (Rokugo, Gunma; Hokiyaake, Nagano; Amagi-yugashima, Shizuoka; Hamazaki, Shizuoka; Nakagawa, Fukui; Kawazu, Shizuoka; Yugawara, Kanagawa; Ashiro, Iwate) and from two other localities (Berufjord, Iceland; Poona, India) do not show extra spots in the diffraction photographs. However, a specimen from another locality in Challis (Rat's Nest, Claim Custer Co., Idaho) showed extra reflections although this locality is quite near the location of the first sample. These results probably indicate different for-

mation conditions between those for the Challis mordenite and mordenites from other localities. The geological significance of the superstructure is, therefore, presently unknown.

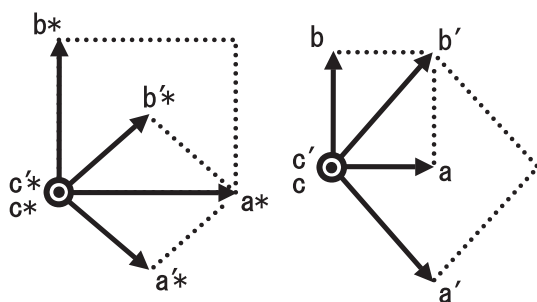
Needle-shaped crystals of mordenite were synthesized under the essentially the same conditions as those reported by Simoncic and Armbruster (2004a). In contrast to the synthesis of Simoncic and Armbruster (2004a), the teflon autoclave (100 mL) was charged with thirteen times the total volume of starting materials and the run duration was extended to seven days at 175° C. One of the crystals ($0.020 \times 0.025 \times 0.140$ mm) was examined by X-ray diffraction methods; however, no additional spots were observed suggesting that the formation condition of the superstructure is more complex.

There have been discussions about the straight T-O-T angle (180°) in the mordenite structure (e.g., Meier 1961; Alberti et al. 1986; Simoncic and Armbruster 2004a), which is energetically unfavorable (Gibbs 1982). The oxygen (O8) shows a large displacement factor perpendicular to the T-O-T axis when the structure is refined in the space group $Cmcm$. To avoid the unfavorable angle, the symmetry reduction from centric $Cmcm$ to acentric $Cmc2_1$ has been proposed (e.g., Alberti et al. 1986).

Our mordenite specimen also shows a large displacement of O8 oxygen (Fig. 5). It is evident that the present superstructure undergoes a symmetry reduction from orthorhombic to monoclinic, which enables the O8 oxygen in the straight T-O-T to decompose into several asymmetric O atoms accommodated in possibly lower symmetrical sites; doubling the volume of superstructure also increases the possibility for the O8 oxygen to occupy different sites. This result decreases the possibility of having the unfavorable 180° T-O-T angle and decomposed O atoms occupy average positions around the O8 oxygen. Thus it is not surprising that the average structure in $Cmcm$, based on the main reflections, shows the high displacement smearing around O8 when mordenite contains superstructure domains. The reduced symmetry (monoclinic from orthorhombic) of the superstructure yields a clue to explain the apparent T-O-T straight extension and the smearing around the O8 oxygen.

The discussions of $c/2$ defects, domains and intergrowths in the structure of mordenite have essentially been based on two experimental observations: (1) diffuse reflections in mordenite have been observed in X-ray and electron diffraction photographs (e.g., Sherman and Bennett 1973; Sanders 1985; Simoncic and Armbruster 2004a; Campbell et al. 2004) and (2) the electron density distributions of framework atoms forming 4-membered rings, have been observed at the positions displaced by $c/2$ in the difference Fourier maps (Mortier et al. 1975; Simoncic and Armbruster 2004a). The diffuse scattering extends perpendicular to the c axis and is restricted for Bragg reflections $l = \text{odd}$. This suggests the presence of linear framework defects displaced by $c/2$ in the structure (Sanders 1985; Campbell and Cheetham 2002; Campbell et al. 2004). The electron density distributions displaced from the framework atoms by $c/2$ proved the presence of some atoms displaced by $c/2$ and suggest two kinds of domain, one displaced from the other by $c/2$, which intergrow in the mordenite structure.

It is emphasized that the extra spots for superstructure are preferentially distributed in the reciprocal planes with $l = \text{odd}$ in this study as shown in Figure 3. It is obvious that this phenomenon in the spot distributions originates from the specific property of the



(a) Reciprocal space (b) Real space

FIGURE 4. Relationship between the unit cells for the basic structure and the superstructure both (a) in the reciprocal space (\mathbf{a}^* , \mathbf{b}^* , and \mathbf{c}^* and \mathbf{a}' , \mathbf{b}' , and \mathbf{c}' , respectively) and (b) in the real space (\mathbf{a} , \mathbf{b} , and \mathbf{c} and \mathbf{a}' , \mathbf{b}' , and \mathbf{c}' , respectively).

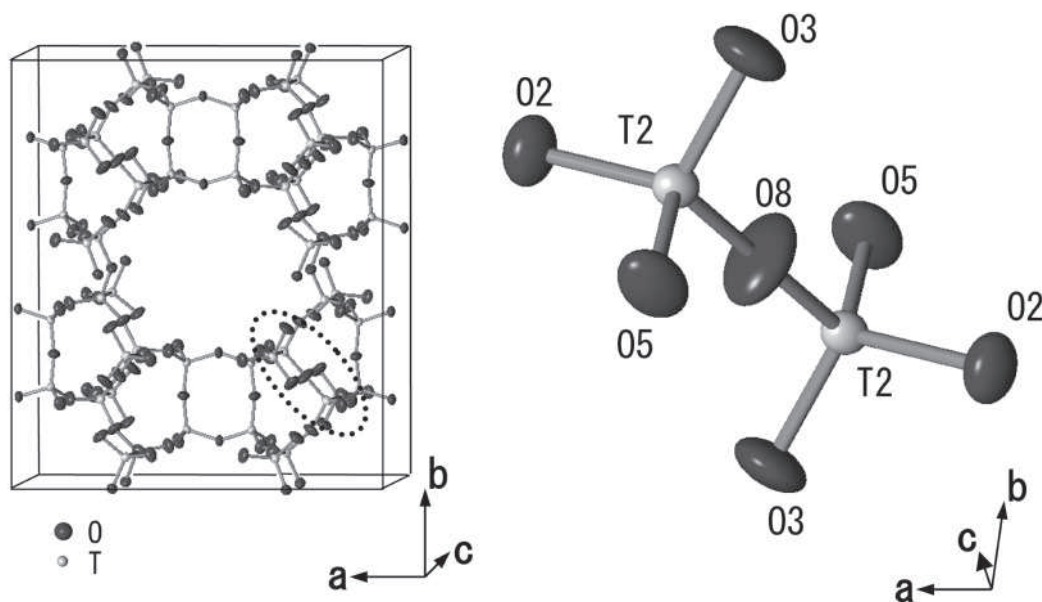


FIGURE 5. The basic structure of mordenite determined from main reflections with $Cmcm$ space group in this study and the magnified straight T2-O8-T2 arrangement. The O8 oxygen shows the large displacement perpendicular to the T-O-T axis.

structure. The extra-spot distributions have the same trend as the diffuse streaks, which are also restricted in the reciprocal layers with $l' = \text{odd}$. This suggests some similarity in the structures, and allows us to propose a model for the superstructure.

The unit cell of the superstructure is made of two basic unit cells (the structure factors, F_1 and F_2), which are equivalent in the $Cmcm$ cell, but differ in the superstructure because of the symmetry reduction and the structural change ($c/2$ displacements). One of these cells is located at the origin and the other at the position $(1/2, 1/2, 0)$ in the unit cell of the superstructure. The framework defects occur at the 4-membered rings, which form columns in the c direction. There are eight columns in the superstructure. If one or several columns are displaced in the c direction by $c/2$, the two structure factors differs from each other slightly since the remaining part, which makes up the major part of cell, remains principally the same. To simplify the discussion, we ignore the modification of the structure originating from the symmetry reduction and assume the difference between the two cells is related only to the $c/2$ displacements of the columns. Here we define the structure factor of the basic unit cell into two parts, unchanged part S and displaced part s in two cells. Note that the displaced part s consists of some of the four 4-membered rings in a basic unit cell. Then, the structure factor of superstructure F' is written as follows:

$$F' = F_1 + [\exp 2\pi i(h'/2 + k'/2)] F_2$$

where

$$F_1 = S + s \text{ and } F_2 = S + [\exp 2\pi i(l'/2)]s.$$

Then,

$$F' = (S + s) + [\exp 2\pi i(h'/2 + k'/2)] \{ S + [\exp 2\pi i(l'/2)]s \} \\ = \{ 1 + [\exp \pi i(h' + k')] \} S + \{ 1 + [\exp \pi i(h' + k' + l')] \} s$$

(1) When $l' = \text{even}$,
 $F' = 2(S + s)$ for $h' + k' = \text{even}$. These reflections superimpose on the main reflections.

$F' = 0$ for $h' + k' = \text{odd}$. These reflections are very weak or absent.

These results demonstrate that extra spots for the superstructure do not separately appear in reciprocal planes with $l' = \text{even}$, except a few weak examples.

(2) When $l' = \text{odd}$,

$F' = 2S$ for $h' + k' = \text{even}$. These reflections superimpose on the main reflections.

$F' = 2s$ for $h' + k' = \text{odd}$. These reflections are independently observed in reciprocal planes with $l' = \text{odd}$.

This explains why the extra spots are observed only on the planes with $l' = \text{odd}$.

This model yields the ordered form for the superstructure with twice the basic unit-cell volume and explains the characteristic spot distributions. It is therefore probable that the $c/2$ linear displacements occur alternatively in the basic unit cells to form a periodic succession.

Campbell et al. (2004) mapped out the distributions of diffuse scattering and demonstrated an excellent consistency with a diffuse scattering pattern simulated from the columnar defects. They claimed that the pattern of broad peaks and nodes resulted from linear columns of framework displaced by $c/2$ with roughly one third of these columnar defects forming stacking faults in the $\{110\}$ planes.

In our study, the diffuse streaks are also seen in layers with $l' = \text{odd}$ as shown in Figure 1c. Judging from all these observations the mordenite consists of domains. The $c/2$ linear displacements are distributed randomly in some parts and form stacking faults and isolated columnar defects, resulting in two kinds of domains A and B (basic and displaced domains both with isolated columnar defects) margined by stacking faults. These domains yield the diffuse streaks as was proposed by Campbell et al. (2004).

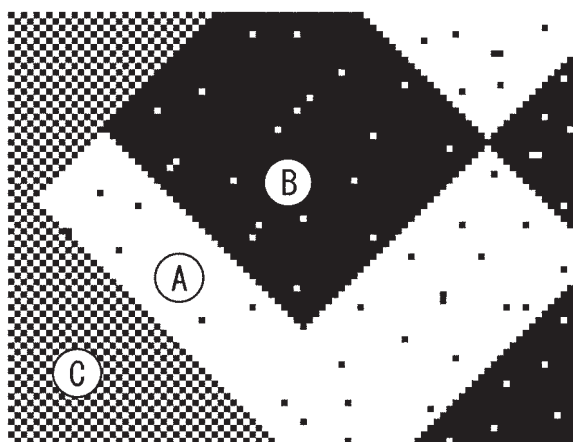


FIGURE 6. The proposed model for two kinds of domains (basic and displaced domains A and B both with isolated columnar defects) and a domain C for the superstructure, based on the distribution of two kinds of basic unit cell, viewed down the c axis. Each pixel of chessboard represents a column of basic unit cell ($a \times b$) size. Each basic unit cell has four columns of 4-membered ring motif defined by Campbell et al. (2004). White pixels differ relatively from black ones in some columnar displacements of 4-membered ring motifs. See the text in detail.

In other parts the displacements are alternatively distributed in an ordered manner to form another kind of domain C (third domain), which yields the superstructure as schematically shown in Figure 6. When this figure is examined more closely, we see the superstructure is composed of the periodic stacking faults in the $\{110\}$ planes, which is consistent with the model for diffuse scattering proposed by Campbell et al. (2004). Our model is essentially the same as one proposed by Campbell et al. (2004) but there is a significant difference. They discussed columnar displacements on the basis of a “4-membered ring motif,” as defined by them, for the origin of the diffuse streaks. The basic unit cell consists of four 4-membered ring motifs. It is shown in this study that the superstructure consists of two basic unit cells and that these two kinds of basic unit cells arrange in an ordered form. Some parts or all the four 4-membered ring motifs in one basic unit cell are displaced from those in the other basic unit cell. The discussed columnar displacements for the superstructure are, therefore, based on the size of the basic unit cell. Correspondingly Figure 6, which shows our model for the superstructure and the three kinds of domains, is drawn on the basis of the basic unit cell rather than on the basis of the linear column of 4-membered ring motifs (each pixel in the figure is the size of $a \times b$). Thus, we conclude that Challis mordenite is composed of the intergrowth of these domains. An effort to solve the superstructure is currently underway and, if successful, will be reported elsewhere.

ACKNOWLEDGMENTS

We are indebted to S. Matsubara and M. Shigeoka of The National Science Museum for their help in kindly giving us some mordenite samples and in analyzing the chemical composition by EPMA, and T. Matsumoto of Kanazawa University

for helpful discussions of space group assignments. We also thank Lanny Ream for aid in collecting the Challis samples. We are grateful to H. Minato of University of Tokyo for motivating the authors to undertake research on cation-exchanged mordenites, which promoted our interest of this specific mineral. The Smithsonian Institution supported our study sending three mordenite specimens from Iceland, India, and New Jersey. We are grateful to H. Ishimoto of Kyoto-Gakuen University for synthesizing mordenite crystals under hydrothermal conditions. Associate editor, Paul Hoskin, and two anonymous reviewers are thanked for their contributions in revising the manuscript.

REFERENCES CITED

- Alberti, A., Davoli, P., and Vezzalini, G. (1986) The crystal structure refinement of a natural mordenite. *Zeitschrift für Kristallographie*, 175, 249–256.
- Armbruster, T. and Gunter, M.E. (2001) Crystal structures of natural zeolites. In D.L. Bish and D.W. Ming, Eds., *Natural Zeolites: Occurrence, Properties, Applications*, 45, 1–67. Reviews in Mineralogy and Geochemistry, Mineralogical Society of America, Chantilly, Virginia.
- Bartelmehs, K.L., Gibbs, G.V., Boisen, M.B. Jr., and Downs, R.T. (1993) Interactive computer software used in teaching and research in mineralogy at Virginia Tech. Geological Society of America Fall Meeting, Boston, A–347.
- Campbell, B.J. and Cheetham, A.K. (2002) Linear framework defects in zeolite mordenite. *Journal of Physical Chemistry B*, 106, 57–62.
- Campbell, B.J., Welberry, T.R., Broach, R.W., Hong, H., and Cheetham, A.K. (2004) Elucidation of zeolite microstructure by synchrotron X-ray diffuse scattering. *Journal of Applied Crystallography*, 37, 187–192.
- Farrugia, L.J. (1999) WinGX suite for small-molecule single-crystal crystallography. *Journal of Applied Crystallography*, 32, 837–838.
- Gibbs, G.V. (1982) Molecules as models for bonding in silicates. *American Mineralogist*, 67, 421–450.
- Kerr, I.S. (1963) Possible structures related to mordenite. *Nature*, 197, 1194–1195.
- Meier, W.M. (1961) The crystal structure of mordenite (ptilolite). *Zeitschrift für Kristallographie*, 115, 439–450.
- Mortier, W.J., Pluth, J.J., and Smith, J.V. (1975) Positions of cations and molecules in zeolites with the mordenite-type framework; II Dehydrated hydrogen-ptilolite. *Materials Research Bulletin*, 10, 1319–1326.
- (1978) Positions of cations and molecules in zeolites with the mordenite-type framework. IV. Dehydrated and rehydrated K-exchanged ptilolite. In L.B. Sand and F.A. Mumpton, Eds., *Natural Zeolites, Occurrence, Properties, Use*, p. 53–76. Pergamon Press, Oxford.
- Otwinowski, Z. and Minor, W. (1997) Processing of X-ray diffraction data collected in oscillation mode. *Methods in Enzymology*, 276, 307–326.
- Ross, C.S. and Shannon, E.V. (1924) Mordenite and associated minerals from near Challis, Custer County, Idaho. *Proceedings of the U.S. National Museum*, 64, art. 19. Smithsonian Institution Press, Washington, D.C.
- Rudolf, P.R. and Garcés, J.M. (1994) Rietveld refinement of several structural models for mordenite that account for differences in the X-ray powder pattern. *Zeolites*, 14, 137–146.
- Sanders, J.V. (1985) Crystallographic faulting in the mordenite group zeolites. *Zeolites*, 5, 81–90.
- Schlenker, J.L., Pluth, J.J., and Smith, J.V. (1978) Positions of cations and molecules in zeolites with the mordenite-type framework; VI Dehydrated barium mordenite. *Materials Research Bulletin*, 13, 169–174.
- (1979) Positions of cations and molecules in zeolites with the mordenite-type framework; VIII Dehydrated sodium-exchanged mordenite. *Materials Research Bulletin*, 14, 751–758.
- Sheldrick, G.M. (1997) SHELXL-97. University of Göttingen, Germany.
- Sherman, J.D. and Bennett, J.M. (1973) Framework structures related to the zeolite mordenite. In W.M. Meier and J.B. Uytterhoeven, Eds., *Molecular Sieves*, p. 52–65. ACS monograph, American Chemical Society, Washington, D.C.
- Simoncic, P. and Armbruster, T. (2004a) Peculiarity and defect structure of the natural and synthetic zeolite mordenite: A single-crystal X-ray study. *American Mineralogist*, 89, 421–431.
- (2004b) Se incorporated into zeolite mordenite-Na: a single-crystal X-ray study. *Microporous and Mesoporous Materials*, 71, 185–198.
- (2005) Cationic methylene blue incorporated into zeolite mordenite-Na: a single crystal X-ray study. *Microporous and Mesoporous Materials*, 81, 87–95.
- Simoncic, P., Armbruster, T., and Pattison, P. (2004) Cationic thionin blue in the channels of zeolite mordenite: a single-crystal X-ray study. *Journal of Physical Chemistry B*, 108, 17352–17360.

MANUSCRIPT RECEIVED JUNE 13, 2006

MANUSCRIPT ACCEPTED DECEMBER 25, 2006

MANUSCRIPT HANDLED BY PAUL HOSKIN